The Astrophysical Journal, 791:114 (11pp), 2014 August 20 doi:10.1088/0004-637X/791/2/114

GJ 832c: A SUPER-EARTH IN THE HABITABLE ZONE*

Robert A. Wittenmyer[1,2,3], Mikko Tuomi[4,5], R. P. Butler[6], H. R. A. Jones[4], Guillem Anglada-Escudé[7], Jonathan Horner[1,2,3], C. G. Tinney[1,2], J. P. Marshall[1,2], B. D. Carter[3], J. Bailey[1,2], G. S. Salter[1,2], S. J. O'Toole[8], D. Wright[1,2], J. D. Crane[9], S. A. Schectman[9], P. Arriagada[6], I. Thompson[9], D. Minniti[10,11,12], J. S. Jenkins[13], and M. Diaz[13]

[1] School of Physics, UNSW Australia, Sydney, NSW 2052, Australia; rob@phys.unsw.edu.au
[2] Australian Centre for Astrobiology, UNSW Australia, Sydney, NSW 2052, Australia
[3] Computational Engineering and Science Research Centre, University of Southern Queensland, Toowoomba, Queensland 4350, Australia
[4] Centre for Astrophysics Research, Science and Technology Research Institute, University of Hertfordshire, College Lane, Hatfield AL10 9AB, UK
[5] Tuorla Observatory, Department of Physics and Astronomy, University of Turku, Väisäläntie 20, FI-21500 Piikkiö, Finland
[6] Department of Terrestrial Magnetism, Carnegie Institution of Washington, 5241 Broad Branch Road, NW, Washington, DC 20015-1305, USA
[7] Astronomy Unit, School of Mathematical Sciences, Queen Mary, University of London, London, UK
[8] Australian Astronomical Observatory, P.O. Box 915, North Ryde, NSW 1670, Australia
[9] The Observatories of the Carnegie Institution of Washington, 813 Santa Barbara Street, Pasadena, CA 91101, USA
[10] Institute of Astrophysics, Pontificia Universidad Catolica de Chile, Casilla 306, Santiago 22, Chile
[11] Vatican Observatory, V00120 Vatican City State, Italy
[12] Departamento de Ciencias Fisicas, Universidad Andres Bello, Republica 220, Santiago, Chile
[13] Departamento de Astronomía, Universidad de Chile, Camino el Observatorio 1515, Casilla 36-D, Las Condes, Santiago, Chile
Received 2014 March 18; accepted 2014 June 20; published 2014 August 5

ABSTRACT

We report the detection of GJ 832c, a super-Earth orbiting near the inner edge of the habitable zone of GJ 832, an M dwarf previously known to host a Jupiter analog in a nearly circular 9.4 yr orbit. The combination of precise radial-velocity measurements from three telescopes reveals the presence of a planet with a period of 35.68 ± 0.03 days and minimum mass ($m \sin i$) of 5.4 ± 1.0 Earth masses. GJ 832c moves on a low-eccentricity orbit ($e = 0.18 \pm 0.13$) toward the inner edge of the habitable zone. However, given the large mass of the planet, it seems likely that it would possess a massive atmosphere, which may well render the planet inhospitable. Indeed, it is perhaps more likely that GJ 832c is a "super-Venus," featuring significant greenhouse forcing. With an outer giant planet and an interior, potentially rocky planet, the GJ 832 planetary system can be thought of as a miniature version of our own solar system.

Key words: astrobiology – planets and satellites: individual (GJ 832) – techniques: radial velocities

Online-only material: color figures

1. INTRODUCTION

For hundreds of years, it was assumed that if planetary systems existed around other stars, they would look substantially like our own solar system (Kant 1755; Laplace & Young 1832). That is, they would feature giant outer planets and rocky inner planets, moving on nearly circular orbits. The discovery of hundreds of extrasolar planetary systems[14] over the last 20 years have instead revealed a picture of planetary system diversity "far stranger than we can imagine" (Haldane 1928). We now know that planetary systems containing a "Jupiter analog" (a gas giant planet that has remained in a low-eccentricity orbit beyond the ice line after planetary migration) are relatively uncommon (Gould et al. 2010; Wittenmyer et al. 2011b, 2014a), while results from the *Kepler* spacecraft (Borucki et al. 2010) have shown us that super-Earths in compact multiple systems are very common (Howard et al. 2012; Batalha et al. 2013; Petigura et al. 2013). While *Kepler* has revolutionized exoplanetary science and provided a first estimate of the frequency of Earth-size planets in Earth-like orbits, long-term radial-velocity surveys (Wittenmyer et al. 2006; Robertson et al. 2012a, 2012b; Zechmeister et al. 2013) complement these data with measurements of the frequency of Jupiter-like planets in Jupiter-like orbits. This in turn will reveal how common solar-system-like architectures are.

In addition to the finding that small, close-in planets are far more common than long-period gas giants (Howard 2013), planet-search efforts are now expanding into new realms of parameter space, seeking to understand how the detailed properties of planetary systems depend on the properties of their host stars. In the early days of exoplanet observations, host stars significantly more massive than our Sun were neglected, due to the difficulties in determining precise radial velocities. In recent years, however, several radial velocity surveys have begun to take advantage of stellar evolution by observing such higher-mass stars once they have evolved off the main sequence to become subgiants and giants. This approach has been successfully used by several teams (e.g., Setiawan et al. 2003; Hatzes et al. 2005; Sato et al. 2005; Johnson et al. 2006; Döllinger et al. 2007; Niedzielski et al. 2009; Wittenmyer et al. 2011a).

Meanwhile, at the low-mass end, M dwarfs are being targeted by a number of near-infrared radial-velocity surveys searching for rocky and potentially habitable planets (e.g., Quirrenbach et al. 2010; Bean et al. 2010; Mahadevan et al. 2012; Barnes et al. 2012; Bonfils et al. 2013a). Notable results from these M-dwarf surveys are that small, rocky planets are common (Bonfils et al. 2013a) and close-in giant planets are rare (Endl et al. 2006); as of yet, there are no robust statistics on the population of longer-period giant planets.

One example of an M dwarf known to host a long-period giant planet is GJ 832. Bailey et al. (2009) reported the discovery by the Anglo-Australian Planet Search (AAPS) of a 0.64 $M_{\rm Jup}$ planet in a nearly circular orbit with period 9.4 ± 0.4 yr.

* This paper includes data gathered with the 6.5 m Magellan Telescopes located at the Las Campanas Observatory, Chile.
[14] The Exoplanet Orbit Database is available at http://exoplanets.org.

The AAPS has been in operation for 15 years and has achieved a long-term radial-velocity precision of 3 m s^{-1} or better since its inception, which is enabling the detection of long-period giant planets (Jones et al. 2010; Wittenmyer et al. 2012b, 2014a). GJ 832b is one of only a handful of such giant planets known to orbit M dwarfs. The others are GJ 179b (Howard et al. 2010), GJ 849b (Butler et al. 2006; Bonfils et al. 2013a), GJ 328b (Robertson et al. 2013), and OGLE-2006-BLG-109Lb (Gaudi et al. 2008; Bennett et al. 2010). Of the long-period giant planets known to orbit M dwarfs, GJ 328b is the one with the largest separation ($a = 4.5 \pm 0.2$ AU). GJ 832b, which lies at $a = 3.4 \pm 0.4$ AU (Bailey et al. 2009), is clearly a Jupiter analog, and may well play a similar dynamical role in the GJ 832 system to that played by Jupiter in our solar system (e.g., Horner & Jones 2008, 2009; Horner et al. 2010).

We report here a second, super-Earth mass planet in the GJ 832 system—with a semimajor axis of $a \sim 0.16$ AU, the GJ 832 system can be considered a miniature solar system analog, with an interior potentially rocky and habitable planet, and a distant gas giant. This paper is organized as follows. Section 2 briefly describes the three data sets and gives the stellar parameters. Section 3 details the traditional and Bayesian orbit fitting procedures and gives the parameters of GJ 832c. In Section 4, we give a discussion on potential habitability before drawing our final conclusions.

2. OBSERVATIONAL DATA

We have combined three high-precision radial-velocity data sets that span a variety of baselines. The data covering the longest baseline (39 epochs over 15 years) were taken by the AAPS team, using the UCLES echelle spectrograph (Diego et al. 1991). An iodine absorption cell provides wavelength calibration from 5000 to 6200 Å. The spectrograph point-spread function (PSF) and wavelength calibration are derived from the absorption lines embedded on the spectrum by the iodine cell (Valenti et al. 1995; Butler et al. 1996). The result is a precise Doppler velocity estimate for each epoch, along with an internal uncertainty estimate, which includes the effects of photon-counting uncertainties, residual errors in the spectrograph PSF model, and variation in the underlying spectrum between the iodine-free template and epoch spectra observed through the iodine cell. All velocities are measured relative to the zero point defined by the template observation. GJ 832 has been observed on 39 epochs since (Table 1), with a total data span of 5465 d (15 years). The mean internal velocity uncertainty for these data is 2.6 m s^{-1}.

GJ 832 has also been observed with the Planet Finder Spectrograph (PFS; Crane et al. 2006, 2008, 2010) on the 6.5 m Magellan II (Clay) Telescope. The PFS is a high-resolution ($R \sim 80{,}000$) echelle spectrograph optimized for high-precision radial-velocity measurements (e.g., Albrecht et al. 2011, 2012; Anglada-Escudé et al. 2012; Arriagada et al. 2013). The PFS also uses the iodine cell method as described above. The 16 measurements of GJ 832 are given in Table 2. The data span 818 days and have a mean internal uncertainty of 0.9 m s^{-1}. A further 54 velocities were obtained from a HARPS-TERRA (Anglada-Escudé & Butler 2012) reduction of the publicly available spectra and and are given in Table 3. The AAPS data are critical for constraining the long-period outer planet, and the extremely precise HARPS and PFS data are necessary for characterizing the inner planet.

To account for possible intrinsic correlations in the radial velocities, we used the same statistical model as Tuomi (2014),

Table 1
AAT/UCLES Radial Velocities for GJ 832

JD-2400000	Velocity (m s^{-1})	Uncertainty (m s^{-1})
51034.08733	7.5	2.2
51119.01595	14.6	6.0
51411.12220	11.4	3.3
51683.26276	18.0	2.8
51743.14564	19.0	2.7
51767.08125	25.0	2.3
52062.24434	19.8	2.2
52092.16771	9.0	2.5
52128.12730	2.2	4.0
52455.23394	0.5	1.6
52477.14549	10.0	2.6
52859.08771	−4.1	2.1
52943.03605	−5.4	2.7
52946.97093	0.5	1.9
53214.20683	−9.5	2.5
53217.21195	−13.9	2.4
53243.05806	−2.1	2.4
53245.15092	−15.4	2.5
53281.04691	−17.3	2.0
53485.30090	−13.1	2.0
53523.30055	−4.9	1.6
53576.14194	−11.5	1.6
53628.06985	−0.4	5.2
53629.05458	−15.2	2.1
53943.10723	−6.3	1.3
54009.03770	−10.4	1.6
54036.95562	−7.2	1.5
54254.19997	3.2	1.8
54371.06683	0.2	1.6
54375.04476	2.5	1.7
54552.29135	8.7	4.0
54553.30430	17.0	2.8
55102.99894	6.4	2.6
55376.26506	9.2	2.5
55430.16511	15.4	2.5
56087.23879	16.1	2.4
56139.24349	14.5	4.6
56467.24320	1.6	3.0
56499.09217	−6.3	4.0

Table 2
Magellan/PFS Radial Velocities for GJ 832

JD-2400000	Velocity (m s^{-1})	Uncertainty (m s^{-1})
55785.64157	0.0	0.9
55787.61821	0.0	0.8
55790.61508	0.3	0.8
55793.63258	0.8	0.9
55795.70095	1.2	0.8
55796.71462	2.5	0.9
55804.66221	0.2	0.9
55844.60440	3.1	0.9
55851.62322	−0.5	0.9
56085.87962	−1.4	0.9
56141.67188	−7.3	0.8
56504.79755	−12.1	1.1
56506.76826	−13.7	1.0
56550.60574	−14.8	0.9
56556.65127	−18.3	1.0
56603.55010	−18.7	0.9

Table 3
HARPS Radial Velocities for GJ 832

JD-2400000	HARPS-TERRA Velocity (m s^{-1})	HARPS-CR Velocity (m s^{-1})	Uncertainty (m s^{-1})
52985.51975	−5.1	−8.4	0.5
53158.90619	−3.1	−6.6	0.6
53205.74533	−5.4	−9.0	0.7
53217.74390	−8.7	−12.4	0.4
53218.70745	−9.3	−12.8	0.2
53229.72411	−6.7	−10.2	0.4
53342.54349	−9.6	−13.3	0.6
53490.92722	−12.1	−16.0	0.8
53491.91352	−7.7	−11.3	1.3
53492.92944	−8.4	−15.1	1.0
53551.85358	−7.8	−11.7	0.3
53573.80021	−11.2	−15.1	0.3
53574.73313	−12.1	−16.9	0.3
53575.73634	−10.4	−14.5	0.3
53576.78382	−11.1	−16.0	0.3
53577.79171	−11.0	−15.1	0.3
53578.74684	−11.9	−15.9	0.3
53579.72975	−11.3	−14.5	0.3
53580.76546	−10.4	−13.8	0.3
53950.81187	−8.6	−12.9	0.4
53974.63508	−6.6	−11.0	0.4
54055.52259	−4.0	−8.4	0.4
54227.91203	−1.2	−5.7	0.4
54228.91277	−1.2	−3.9	0.4
54230.88177	−0.3	−3.4	0.4
54233.92916	−0.1	−3.9	0.7
54234.92383	0.0	−4.0	0.4
54255.84319	1.7	−2.9	0.4
54257.88296	1.7	−3.4	0.4
54258.91849	0.8	−3.9	0.4
54291.81785	2.6	−2.0	0.5
54293.78153	3.4	−1.6	0.3
54295.82951	4.4	−0.5	0.4
54299.83521	6.9	2.0	0.7
54314.77282	2.4	−2.4	0.4
54316.60452	1.0	−4.5	0.2
54319.80379	0.7	−4.2	0.4
54339.64829	5.2	0.5	0.2
54341.76270	5.9	1.1	0.3
54342.67095	3.0	−2.7	0.1
54347.71453	0.0	−4.4	0.3
54349.72920	0.8	−2.6	0.4
54387.61499	4.0	−0.7	0.1
54393.60450	3.6	−1.3	0.4
54420.51798	2.4	−2.4	0.3
54426.51760	3.4	−1.0	0.3
54446.53786	9.5	4.7	0.5
54451.53099	9.5	4.5	0.5
54453.53428	7.1	1.1	0.2
54464.53844	6.2	1.3	0.5
54639.91552	10.7	5.7	0.3
54658.87484	15.7	10.7	0.6
54662.86973	14.5	9.3	0.2
54704.70377	11.6	6.5	0.5

which assumes that the deviation of the ith measurement of a given instrument from the mean depends also on the deviation of the previous measurement. In other words, these deviations are correlated with a correlation coefficient of $\phi \exp\{-(t_i - t_{i-1})/\tau\}$ that decreases exponentially as the gap between the two measurements (the difference $t_i - t_{i-1}$) increases. We set the correlation timescale such that $\tau = 4$ days (Baluev 2013; Tuomi et al. 2014). Parameter $\phi \in [-1, 1]$ is a free parameter in the model of Tuomi et al. (2014). The maximum a posteriori estimates of these "nuisance parameters" are given in Table 4. Only for the HARPS-TERRA data does the correlation coefficient ϕ differ significantly from zero. We thus consider an additional data set in our analysis, "HARPS-CR," which has been corrected for these intrinsic correlations. Those data are also shown in Table 3.

Table 4
Maximum A Posteriori Estimates and 99% Credibility Intervals for the Nuisance Parameters: Reference Velocities with Respect to the Data Mean (γ), Excess White Noise (σ), and Intrinsic Correlation (ϕ)

Parameter	HARPS	PFS	UCLES
γ	4.56 [−1.83, 11.63]	−6.64 [−17.20, 3.91]	1.14 [−5.52, 7.80]
σ	1.33 [0.90, 1.91]	1.45 [0.44, 2.99]	4.66 [3.13, 6.15]
ϕ	0.90 [0.25, 1]	0.77 [−1,1]	0.11 [−0.30, 0.57]

Table 5
Stellar Parameters for GJ 832

Parameter	Value	Reference
Spec. Type	M1.5	Gray et al. (2006)
	M1V	Jenkins et al. (2006)
Mass ($M_\odot$)	0.45	Bonfils et al. (2013a)
	0.45 ± 0.05	Bailey et al. (2009)
Distance (pc)	4.95 ± 0.03	van Leeuwen (2007)
$\log R'_{HK}$	−5.10	Jenkins et al. (2006)
(Fe/H)	-0.3 ± 0.2	Bonfils et al. (2013a)
	−0.7	Schiavon et al. (1997)
$T_{\rm eff}$ (K)	3472	Casagrande et al. (2008)
Luminosity ($L_\odot$)	0.020	Boyajian et al. (2012)
	0.026	Bonfils et al. (2013a)
log g	4.7	Schiavon et al. (1997)

3. ORBIT FITTING AND PLANETARY PARAMETERS

GJ 832 (HD 204961, HIP 106440, LHS 3685) is a very nearby M1.5 dwarf, lying at 4.95 pc (van Leeuwen 2007). The parameters of the host star are summarized in Table 5. While the original discovery paper for the giant planet (Bailey et al. 2009) did not note any residual signals of interest, Bonfils et al. (2013a) combined AAT ($N = 32$) and HARPS ($N = 54$) data to refine the planet's orbital parameters and mentioned a potential 35 day residual periodicity. They concluded that the data in hand did not yet warrant a secure detection as the false-alarm probability (FAP) exceeded 1%. The AAT data published in Bailey et al. (2009) contained 32 epochs spanning 3519 days (9.6 years). Combining all available data, we now have 109 epochs covering a 15 year baseline, enabling us to better characterize the long-period planet and increasing our sensitivity to any residual signals of interest.

3.1. Bayesian Approach

We analyzed the combined HARPS, PFS, and UCLES radial velocities in several stages. First, we drew a sample from the posterior density of a model without Keplerian signals, i.e., a model with $k = 0$, by using the adaptive Metropolis algorithm (Haario et al. 2001). This is a generalization of the Metropolis–Hastings Markov chain Monte Carlo technique (Metropolis et al. 1953; Hastings 1970) that adapts the proposal density to the information gathered from the posterior. This baseline model enabled us to determine whether the models with $k = 1, 2, ...n$ Keplerian signals were, statistically, significantly

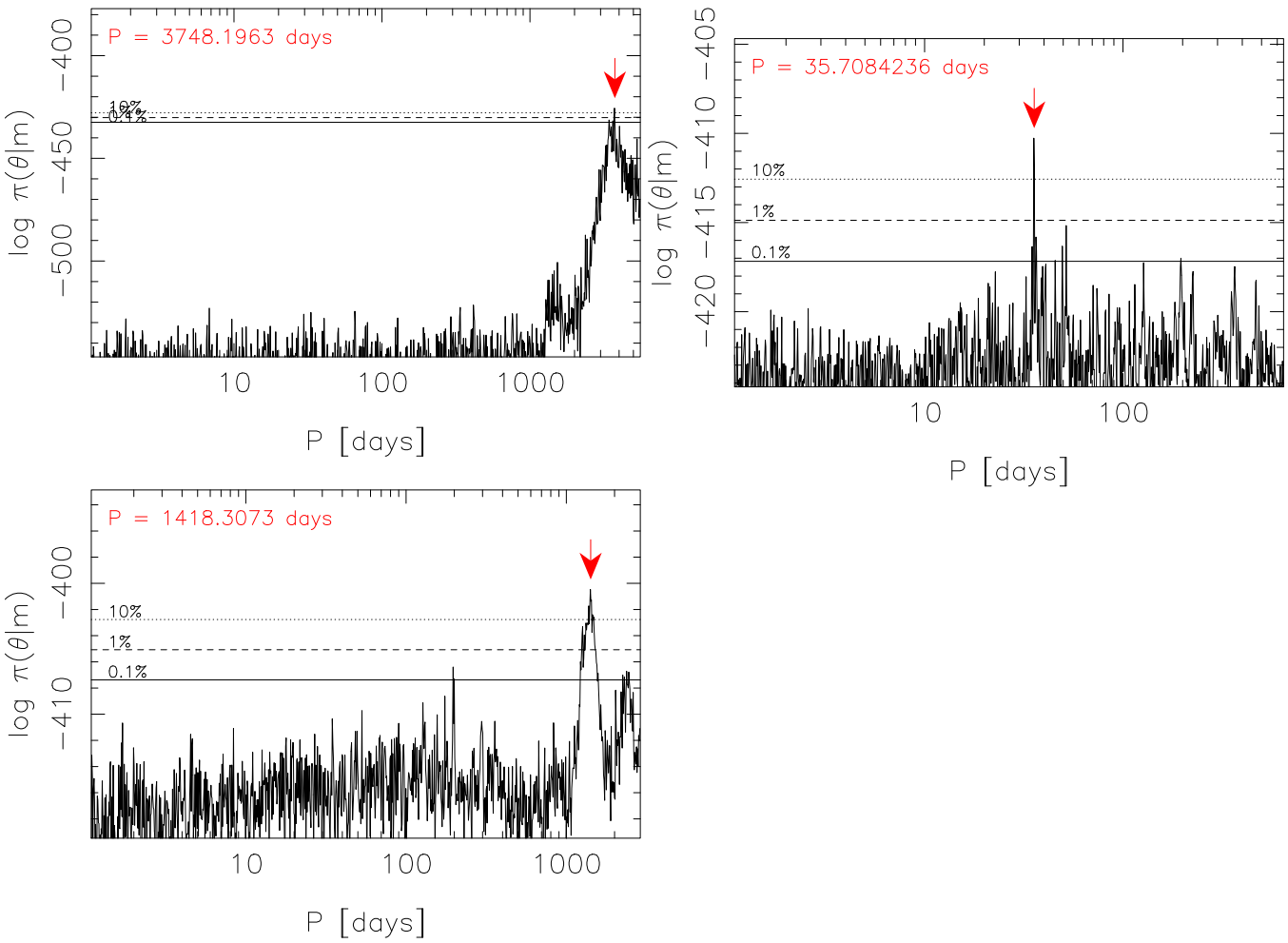

Figure 1. Estimated posterior density of the period of the Keplerian signals based on MCMC sampling. The red arrow indicates the global maximum identified by the chain and the horizontal lines denote the 10% (dotted), 1% (dashed), and 0.1% (solid) probability thresholds with respect to the maximum. Top panel: GJ 832b. Middle panel: GJ 832c. Bottom panel: residuals to two-planet fit; this periodicity did not meet our criteria for a significant detection.

(A color version of this figure is available in the online journal.)

better descriptions of the data by estimating the Bayesian evidence ratios of the different models (e.g., Kass & Raftery 1995; Tuomi 2014; Tuomi et al. 2014). For this purpose, we used the simple estimate described in Newton & Raftery (1994).

The search for periodic signals in the data was performed by using tempered samplings (Tuomi & Anglada-Escudé 2013; Tuomi 2014; Tuomi et al. 2014) such that a scaled likelihood $l(m|\theta)^{\beta}$ and a scaled prior density $\pi(\theta)^{\beta}$, where m is the measurements and θ the parameter vector, instead of the common likelihood $l(m|\theta)$ and prior $\pi\theta$. We choose $\beta \in (0, 1)$ low enough such that the posterior probability density is scaled sufficiently to enable the Markov chains to visit repeatedly all relevant areas in the parameter space, in particular, the period space. In this way, we can estimate the general shape of the posterior density as a function of the period parameter to see which periods correspond to the highest probability maxima. This is not necessarily possible with "normal" samplings (i.e., when $\beta = 1$) because one or some of the maxima in the period space could be so high and significant that the Markov chains fail to visit the whole period space efficiently due to the samplings getting "stuck" in one of the corresponding maxima. This could happen because the parameter space around some maxima is in practice so much less probable that any proposed values outside the maximum are rejected in the MCMC sampling. The application of such tempered samplings thus enables an efficient search for periodicities in the data.

We maximized parameter $\beta \in (0, 1)$ such that the period parameter visited all areas in the period space between one day and the data baseline during these tempered samplings. The results from this period search reveal the shape of the posterior probability density as a function of period (see Figure 1). This enabled us to identify all relevant maxima in the period space because such transformation artificially decreases the significances of the maxima, while leaving their locations unchanged. To ensure that the Markov chains visited all areas of high posterior probability in the parameter space, and especially through the period space, we applied the delayed-rejection adaptive-Metropolis algorithm (Haario et al. 2006), where another proposed parameter vector from a narrower proposal density is tested if the first proposed vector is rejected. This enables an efficient periodicity search because the chains visit the narrow probability maxima in the period space. One such sampling is shown in the middle panel of Figure 1 when searching for a second periodicity in the data. The chain clearly identifies a global maximum at a period of 35.7 days.

After such tempered samplings, we started several "cold chains," i.e., normal chains such that $\beta = 1$, in the vicinity of the highest maxima to determine which of them were significant

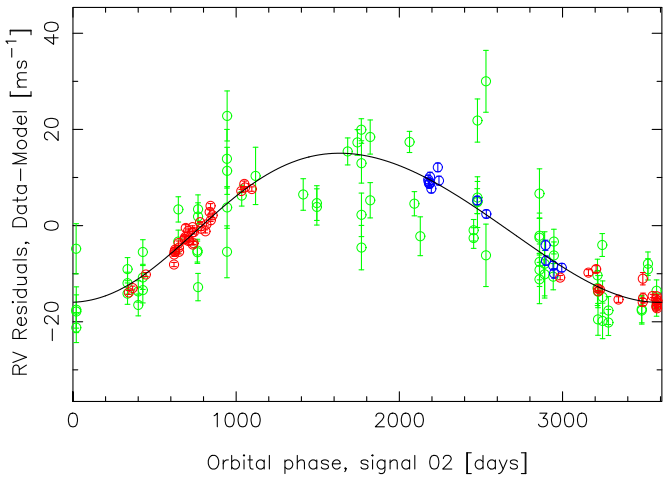

Figure 2. Radial velocities and fit for GJ 832b; the signal of the second planet has been removed. AAT (green), HARPS (red), PFS (blue).

(A color version of this figure is available in the online journal.)

Table 6
Maximum A Posteriori Estimates and 99% Credibility Intervals of the Keplerian Parameters and the Linear Trend $\dot{\gamma}$

Parameter	GJ 832b	GJ 832c
P (days)	3660 [3400, 3970]	35.67 [35.55, 35.82]
K (ms^{-1})	15.51 [13.47, 17.36]	1.62 [0.70, 2.56]
e	0.08 [0, 0.17]	0.03 [0, 0.25]
ω (deg)	246 [149, 304]	80 [0, 360]
Mean anomaly[a] (deg)	40 [315, 109]	246 [0, 360]
a (AU)	3.60 [3.18, 3.96]	0.162 [0.145, 0.179]
$m \sin i$ ($M_\oplus$)	219 [168, 270]	5.0 [1.9, 8.1]
$\dot{\gamma}$ (ms^{-1}yr^{-1})	0.18 [−0.46, 0.69]	
γ_{HARPS}	4.56 [−1.83, 11.63]	
γ_{PFS}	−6.64 [−17.20, 3.91]	
γ_{AAT}	1.14 [−5.52, 7.80]	

Note. [a] Computed for epoch JD = 2450000.0.

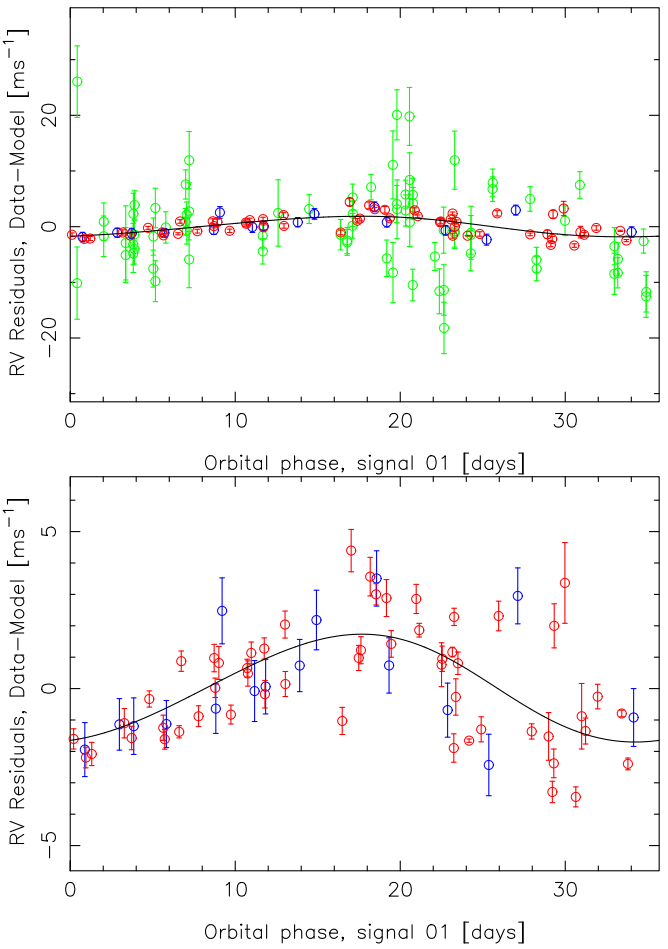

Figure 3. Top: radial velocities and fit for GJ 832c; the signal of the outer planet has been removed. AAT (green), HARPS (red), PFS (blue). Bottom: same as top panel, but the AAT data have been omitted from the plot to more clearly show the low-amplitude signal.

(A color version of this figure is available in the online journal.)

Table 7
Correlations of GJ 832 Velocities with Activity Indicators

Indicator	MAP estimate	99% confidence interval
BIS	−0.21	[−0.66, 0.14]
FWHM	−0.04	[−0.10, 0.04]
S-index (m^{-1}s^{-1}dex)	1.5	[−8.2, 11.0]

according to the detection criteria discussed in Tuomi (2014) and Tuomi et al. (2014). The statistical significance of a signal is quantified by the Bayesian evidence ratio $B(k, k-1)$. We required that the Bayesian evidence ratio be at least 10^4 times greater for a model with $k+1$ than for a model with k signals to state that there are $k+1$ signals present in the data. That is, the model with the signal must be 10,000 times more probable than the model without. For the combination of the three data sets considered here, we obtain $B(1, 0) = 4.5 \times 10^{60}$ (in favor of a one-planet model over zero planets). The 35 day signal is also significant with respect to our detection threshold as it is detected with $B(2, 1) = 6.6 \times 10^5$. The maximum a posteriori estimates of the model parameters, together with the corresponding Bayesian 99% credibility intervals, are listed in Table 6. The data and best-fit models are shown in Figure 2 (GJ 832b) and Figure 3 (GJ 832c).

In addition to the velocities, various activity indices are also available for the epochs of the GJ 832 HARPS observations (Bonfils et al. 2013a). Those metrics, derived from the cross-correlation function (CCF) are the bisector inverse slope (BIS), described fully in Queloz et al. (2001), and the CCF FWHM. We modeled correlations of the HARPS-TERRA velocities with BIS, FWHM, and S index by assuming these correlations were linear, which represents the first-order approximation for such dependence. However, accounting for these correlations did not improve the model, which indicates that such linear correlations were insignificant. Furthermore, when we computed the best-fit estimates for such linear correlation parameters, they were all consistent with zero, as shown in Table 7.

3.2. Traditional Approach

The combination of three data sets with high precision and long observational baseline yields evidence for a second, low-mass planet orbiting GJ 832. Given that we have used data from every telescope which is able to achieve sufficient velocity precision for this Southern M dwarf ($\delta = -49.^\circ0$), independent confirmation of GJ 832c is problematic. It is prudent, then, to employ an independent analysis to test the plausibility of the 35 day signal.

For this analysis, we use the HARPS data set which has been corrected for intrinsic correlations as described above—labeled

Table 8
Characteristics of Two-planet Fits for GJ 832

	AAT rms (m s^{-1})	HARPS-TERRA rms (m s^{-1})	HARPS-CR rms (m s^{-1})	PFS rms (m s^{-1})	Total rms (m s^{-1})	χ^2_ν
Fit 1	5.66	1.53	···	1.60	3.57	1.206
Fit 2	5.63	···	1.40	1.55	3.53	1.080

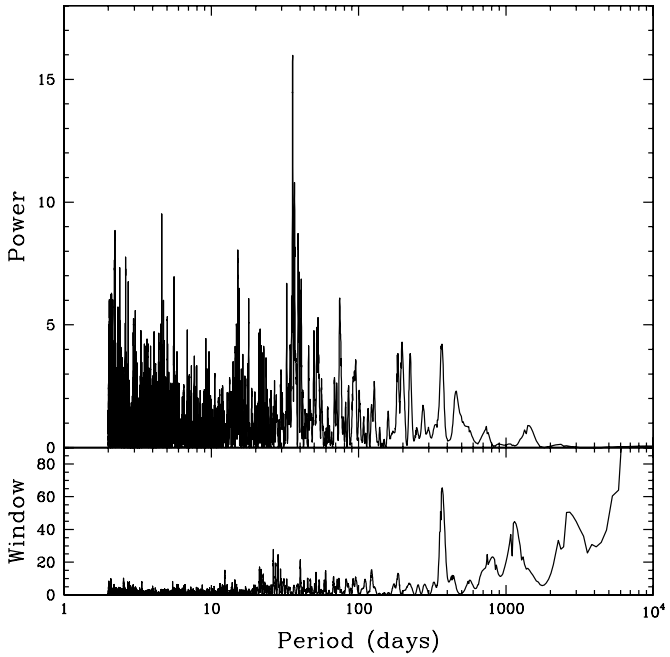

Figure 4. Generalized Lomb–Scargle periodogram of the residuals to a single-planet fit for GJ 832. A strong peak at 35.67 days is present, with a bootstrap FAP of 0.04%.

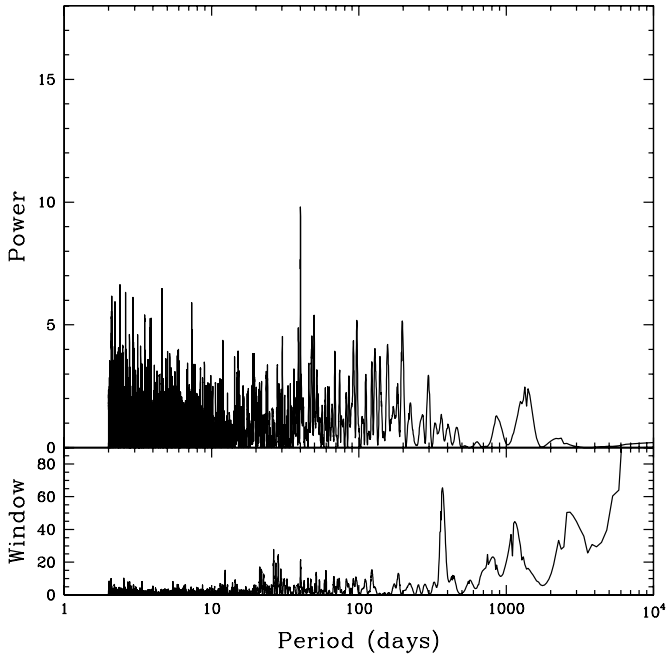

Figure 5. Generalized Lomb–Scargle periodogram of the residuals to the two-planet fit for GJ 832. All three data sets are included. The peak at 40 days has a bootstrap FAP of 4.56%, 100 times less significant than the peak due to the inner planet (Figure 4).

here as "HARPS-CR." An instrumental noise term was derived from the excess white noise parameter given in Table 4—HARPS-CR: 1.33 m s^{-1}, PFS: 1.45 m s^{-1}, AAT: 4.66 m s^{-1}. Before orbit fitting, that noise was added in quadrature to the uncertainties of each data point. We repeated our analysis using the unaltered HARPS-TERRA velocities, and we found throughout that the HARPS-CR and HARPS-TERRA data sets gave the same results.

First, we fit a single-planet model to the three data sets using the nonlinear least-squares minimization routine *GaussFit* (Jefferys et al. 1988). The velocity offsets between the three data sets were included as free parameters. The rms scatter about the three data sets are as follows—AAT: 5.72 m s^{-1}, HARPS-CR: 1.88 m s^{-1}, PFS: 1.74 m s^{-1}. We performed a periodogram search on the residuals to the one-planet fit, using the generalized Lomb–Scargle formalism of Zechmeister & Kürster (2009). Unlike the classical Lomb–Scargle periodogram (Lomb 1976; Scargle 1982), this technique accounts for the uncertainties on the individual data points, which is critically important for the case of GJ 832 where we have combined data sets with significantly different precisions. The periodogram of the one-planet fit is shown in Figure 4; the highest peak is at 35.67 days. The FAP was estimated using a bootstrap randomization method (Kürster et al. 1997). From 10,000 bootstrap realizations, the 35.67 day peak is shown to be highly significant, with FAP = 0.0004 (0.04%).

We then used a genetic algorithm to search a wide parameter space for two-planet models and to check that any candidate secondary signal is indeed the global best fit. Our group has used this approach extensively (e.g., Tinney et al. 2011; Wittenmyer et al. 2012a, 2014b) when the orbital parameters of a planet candidate are highly uncertain. We allowed the genetic algorithm to fit two-Keplerian models to the three data sets simultaneously, searching secondary periods from 10 to 3000 days. It ran for 50,000 iterations, testing a total of about 10^7 possible two-Keplerian configurations. The genetic algorithm converged on $P_2 \sim 35$ days, giving confidence that this is the most likely period for a candidate second planet.

We then obtained a final two-planet fit using *GaussFit*. Again, we performed the fit twice, using the two versions of the HARPS velocities. The details of each fit are summarized in Table 8. Both fits gave the same results, though the HARPS-CR set ("Fit 2") gave a slightly better rms and smaller uncertainties on the planetary parameters; hence, we adopt those results in Table 9. These fits reveal a second planet, GJ 832c, with $P = 35.68 \pm 0.03$ d and $m \sin i = 5.40 \pm 0.95\ M_\oplus$ on a nearly circular orbit. A periodogram of the residuals to the two-planet fit is shown in Figure 5; the highest peak at 40.2 days has a bootstrap FAP of 0.0456 (4.6%).

4. DISCUSSION AND CONCLUSIONS

4.1. Testing the Planet Hypothesis

If the 35 day signal is real, adding data should result in a higher significance level, i.e., a lower FAP determined by the bootstrap

Table 9
Least-squares Keplerian Orbital Solutions for the GJ 832 Planetary System

Parameter	GJ 832b	GJ 832c
P (days)	3657 [3553, 3761]	35.68 [35.65, 35.71]
K ($m\,s^{-1}$)	15.4 [14.7, 16.1]	1.79 [1.52, 2.06]
e	0.08 [0.02, 0.10]	0.18 [0.05, 0.31]
ω (deg)	246 [224, 268]	10 [323, 57]
Mean anomaly[a] (deg)	307 [285, 330]	165 [112, 218]
a (AU)	3.56 [3.28, 3.84]	0.163 [0.157, 0.169]
$m \sin i$ ($M_\oplus$)	216 [188, 245]	5.40 [4.45, 6.35]
$\dot{\gamma}$ ($ms^{-1}yr^{-1}$)	0.0 (fixed)	
γ_{HARPS}	1.05 [0.27, 1.83]	
γ_{PFS}	−9.35 [−11.07, −7.63]	
γ_{AAT}	3.08 [2.19, 3.96]	

Note. Uncertainties are given as a $\pm 1\sigma$ range.
[a] Computed for epoch JD = 2450000.0.

method described above (Kürster et al. 1997). We test this by performing one-planet fits on various combinations of the three data sets considered here. In these fits, the parameters of the outer planet are started at the best-fit values in Table 10 but are allowed to vary. For data combinations with insufficient time baselines to adequately fit the outer planet, its parameters are instead fixed at their best-fit values. After each fit, we removed the signal of the outer planet, examined the periodogram (Zechmeister & Kürster 2009) of the residuals, and computed the FAP of the highest remaining peak using 10,000 bootstrap randomizations. The results are summarized in Table 10. The AAT data alone are not sufficiently precise to detect the $K \lesssim 2$ m s^{-1} signal of the candidate planet, nor did the addition of only 16 epochs from PFS enable the detection of any significant residual signals. Nevertheless, we see in Table 10 that the addition of data indeed strengthens the significance of the 35.6 day signal, adding confidence that the signal is real and not an artifact of one particular instrument. Table 10 also indicates that the HARPS data are necessary to pull out the signal of GJ 832c, and the AAT data, while noisy, are necessary for constraining the outer planet.

The next obvious question to ask is whether the detected signal is intrinsic to the star. As noted in Bonfils et al. (2013a) and in Section 3.1, the HARPS planet-search programs use the additional diagnostics BIS and CCF-FWHM to check for star-induced variability. Being contemporaneous with the velocity measurements, both of these measures can be directly compared with the velocity derived from a given spectrum. If BIS or FWHM show correlations with the velocities, a candidate radial-velocity signal can be considered suspect. Figure 6 plots the HARPS velocities (after removing the outer planet) against the BIS (left panel) and the CCF FWHM (right panel). No correlations are evident, and the highest BIS periodogram peak at 179.6 days has a bootstrap FAP of 17%. For FWHM, the highest periodogram peak at 6322 days has a bootstrap FAP $< 0.01\%$. For comparison, the outer planet has a period of 3660 days, and the HARPS FWHM data only span 1719 days; for these reasons, we maintain the conclusion of Bailey et al. (2009) that the long-period velocity signal is due to an orbiting body. As shown in Table 7, none of these activity indicators had correlations significantly different from zero. These results are further evidence that the 35.6 day signal is not intrinsic to the star.

4.2. GJ 832c: a Habitable-zone Super-Earth

In recent years, a growing number of super-Earths have been discovered that orbit their host stars at a distance that may be compatible with the existence of liquid water somewhere on the planet were it to have a surface (i.e.,within the classical habitable zone). A list of these planets is given in Table 11. Of those planets, perhaps the most interesting are those orbiting GJ 581. In that system, a total of six planets have been claimed, although at least two of these are still the subject of significant debate (e.g., Mayor et al. 2009; Vogt et al. 2010; Tuomi 2011; von Braun et al. 2011; Tadeu dos Santos et al. 2012; Vogt et al. 2012; Baluev 2013). The proposed planetary system around GJ 581 displays an orbital architecture that is strikingly similar to a miniature version of our own solar system. The similarity to our own solar system has recently been enhanced by the results of the DEBRIS survey (Matthews et al. 2010), which recently discovered and spatially resolved a disk of debris orbiting GJ 581 (Lestrade et al. 2012), analogous to the solar system's Edgeworth–Kuiper belt.

We can estimate the location of the classical habitable zone following the prescriptions given in Selsis et al. (2007) and Kopparapu et al. (2014), using the stellar parameters detailed in Table 5. In both cases, we find that GJ 832c lies just inside the inner edge of the potentially habitable region—with the Selsis et al. prescription yielding a habitable zone that stretches between 0.13 and 0.28 au, and the Kopparapu et al. prescription suggesting that the conservative habitable zone for a 5 $M_\oplus$ planet lies between 0.130 and 0.237 au, compared to the measured $a = 0.163 \pm 0.006$ au for GJ 832c.

Although GJ 832c is sufficiently far from its host star that there is the potential for liquid water to exist on its surface, this does not necessarily make that planet truly habitable. Indeed, there is a vast number of factors that can contribute to the habitability of a given exoplanet beyond the distance at which it orbits its host star (e.g., Horner & Jones 2010; Horner 2014). Given the planet's proximity to its host star, it seems likely that GJ 832 c will be trapped in a spin-orbit resonance, though moderate orbital eccentricity may mean it is not necessarily trapped in a resonance that causes one side of the planet to

Table 10
FAP of Residual Signal after Removing GJ 832b

Data Used	N	Period (days)	FAP	Data Used	N	Period (days)	FAP
AAT	39	2.77	0.1481				
AAT + PFS	55	15.38	0.7279				
HARPS-TERRA[a]	54	40.5	0.0066	HARPS-CR[a]	54	35.6	0.0017
HARPS-TERRA + PFS[a]	70	35.66	0.0331	HARPS-CR + PFS[a]	70	35.66	<0.0001
AAT + HARPS-TERRA	93	35.6	0.0461	AAT + HARPS-CR	93	35.7	0.0014
AAT + HARPS-TERRA + PFS	109	35.7	0.0164	AAT + HARPS-CR + PFS	109	35.7	0.0004

Note. [a] Parameters of GJ 832b held fixed at best-fit values in Table 9.

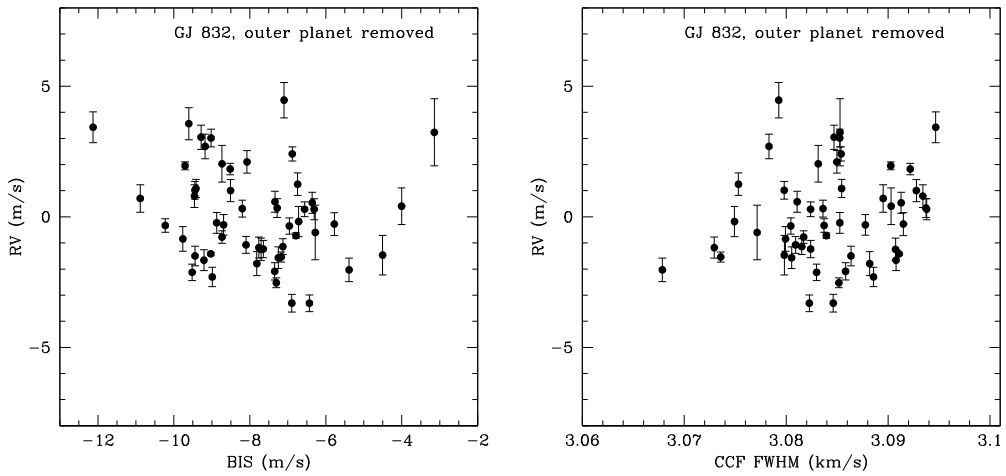

Figure 6. HARPS radial velocities (after removing the signal of GJ 832b) vs. the bisector inverse slope (BIS; left panel) and the FWHM of the cross-correlation function (CCF FWHM; right panel). No correlations are evident, supporting the hypothesis that the 35.6 day signal is due to an orbiting planet.

Table 11
Candidate Habitable-zone Exoplanets

Planet[a]	Mass[b] ($M_\oplus$)	Semimajor axis (AU)	HZ range[c] (AU)	Eccentricity	References[d]
GJ 163c	6.8 ± 0.9	0.1254 ± 0.0001	0.134–0.237	0.099 ± 0.086	1, 2
GJ 581g[e]	2.242 ± 0.644	0.13386 ± 0.00173	0.095–0.168	0.0	3, 4, 5, 6, 7, 8, 9
GJ 581d	5.94 ± 1.05	0.21778 ± 0.00198	0.095–0.168	0.0	8
GJ 667Cc	3.8 [2.6, 6.3]	0.125 [0.112, 0.137]	0.118–0.231	0.02 [0, 0.17]	10, 11, 12, 13
GJ 667Cf	2.7 [1.5, 4.1]	0.156 [0.139, 0.170]	0.118–0.231	0.03 [0, 0.19]	
GJ 667Ce	2.7 [1.3, 4.3]	0.213 [0.191, 0.232]	0.118–0.231	0.02 [0, 0.24]	
GJ 832c	5.406 ± 0.954	0.163 ± 0.006	0.130–0.237	0.18 ± 0.13	This work
HD 40307g	7.1 [4.5, 9.7]	0.600 [0.567, 0.634]	0.476–0.863	0.29 [0, 0.60]	14
Kepler-22b	<36 (1σ)	$0.849^{+0.018}_{-0.017}$	0.858–1.524	...	15, 16
Kepler-61b	...	0.2575 ± 0.005	0.295–0.561	$0.0^{+0.25}_{-0.0}$	17, 18
Kepler-62e	<36 (95%)	0.427 ± 0.004	0.457–0.833	0.13 ± 0.112	17, 19
Kepler-62f	<35 (95%)	0.718 ± 0.007	0.457–0.833	0.0944 ± 0.021	
Kepler-174d	...	0.677	...	0.431–0.786	20
Kepler-296f	...	0.263	...	0.143–0.277	20
Kepler-298d	...	0.305	...	0.351–0.65	20
Kepler-309c	...	0.401	...	0.228–0.434	20

Notes.
[a] Planet data from the Exoplanet Orbit Database at http://exoplanets.org.
[b] Uncertainties given in square brackets refer to the 99% credibility intervals on the value in question, while those given as $\pm$ refer to the 1σ uncertainty.
[c] Conservative habitable-zone limits computed after Kopparapu et al. (2014) and http://www3.geosc.psu.edu/~ruk15/planets/
[d] **References.** (1) Bonfils et al. 2013b; (2) Mayor et al. 2009; (3) Vogt et al. 2010; (4) Tuomi 2011; (5) von Braun et al. 2011; (6) Tadeu dos Santos et al. 2012; (7) Vogt et al. 2012; (8) Lestrade et al. 2012; (9) Anglada-Escudé et al. 2012; (10) Anglada-Escudé et al. 2013; (11) Delfosse et al. 2013; (12) Makarov & Berghea 2014; (13) Tuomi et al. 2013a; (14) Borucki et al. 2012; (15) Neubauer et al. 2012; (16) Borucki et al. 2011; (17) Ballard et al. 2013; (18) Borucki et al. 2013; (19) Rowe et al. 2014.
[e] For the purposes of this table, we list the cirular five-planet model for GJ 581 given in Vogt et al. (2012).

perpetually face towards the Sun. In our own solar system, the planet Mercury is trapped in such a resonance: rotating three times on its axis in the time it takes to complete two full orbits of the Sun. Mercury's capture to that particular resonance is almost certainly the result of its relatively eccentric orbit (e.g., Correia & Laskar 2009)—and so it is certainly feasible that GJ 832 c, while tidally locked, is not trapped in 1:1 spin-orbit resonance. Even if the planet is trapped in such a resonance, however, that might not be deleterious to the prospects for its being habitable. For example, recent work by Yang et al. (2014), employing a three-dimensional general circulation model, suggests that planets with slower rotation rates would be able to remain habitable at higher flux levels than for comparable, rapidly rotating planets.

Given the planet's large mass, however, it is likely to be shrouded in a dense atmosphere, which might in turn render it an uninhabitable "super-Venus" (see Kane et al. 2013 for a discussion on this class of planet in the Kepler-69 system). In that scenario, the dense atmosphere would provide a strong greenhouse effect, raising the surface temperature enough to cause any oceans to boil away, as is thought to have happened to Venus early in the lifetime of the solar system (e.g., Kasting 1988). Kasting et al. (1993) proposed that tidally locked planets around late-type stars might be rendered uninhabitable by atmospheric freeze-out if they were locked in a 1:1 spin-orbit resonance. However, such a massive atmosphere would also be able to prevent the freeze out of the planet's atmosphere if it were trapped in a 1:1 spin-orbit resonance (Heath et al. 1999).

A detailed review of the potential habitability of planets around M dwarfs by Tarter et al. (2007) re-opened the possibility of habitability for such planets. More recently, Kopparapu et al. (2014) have argued that the inner edge of the habitable zone moves inward for more massive planets—a scenario which would operate in favor of GJ 832c's habitability.

Given the large mass of GJ 832c and the high probability of it having a thick, dense atmosphere, it is reasonable to assume that it is unlikely to be a habitable planet. However, it is natural to ask whether it could host a giant satellite, which might itself be habitable. Speculation about habitable exomoons is not a new thing, and in recent years, a number of papers have been published discussing the prospects for such satellites orbiting a variety of newly discovered planets—e.g., the gas giants HD 38283b (Tinney et al. 2011) and HD 23079b (Cuntz et al. 2013) and the super-Earth Kepler-22b (Kipping et al. 2013)—or discussing the viability of such satellites as potential locations for life in a more general sense (e.g., Heller 2012; Forgan & Kipping 2013; Heller & Barnes 2013). As such, it is interesting to consider whether GJ 832c could host such a potentially habitable satellite, although we acknowledge that the detection of such a satellite is currently well beyond our means.

Within our solar system, one planet (the Earth) and several of the minor bodies (such as Pluto) are known to have giant satellites that are thought to have formed as a result of giant impacts on their host object toward the end of planet formation (e.g., Benz et al. 1986; Canup 2004, Canup 2005). In the case of the Pluto–Charon binary, the mass of Charon is approximately one-ninth that of Pluto—were that extrapolated to the case of GJ 832c, it would result in a moon somewhat greater than one-half of the mass of the Earth.[15] However, could GJ 832c retain such a satellite while orbiting so close to its host star?

The Hill sphere of an object is the region in which its gravitational pull on a satellite (or passing object) would dominate over that from any other object. Typically, within our solar system, the regular satellites of the planets orbit their hosts well within their Hill sphere. Our Moon, for example, orbits at approximately one-quarter of the Hill radius. For GJ 832c, assuming a mass of 5.406 times that of the Earth, and a host-star mass of 0.45 $M_{\odot}$, the Hill radius would be just 0.00306 au, or 460,000 km. In and of itself, this result does not seem to preclude the existence of a habitable exomoon orbiting GJ 832c. However, Cuntz et al. (2013) found that for the case of the gas giant planet HD 23079b, satellites on prograde orbits were only stable out to a distance of approximately 0.3 Hill radii—a result that compares relatively well to the orbital distance of the Moon, which currently orbits Earth at a distance of ∼0.25 Hill radii. Were the same true for the case of GJ 832c, this would reduce the region of stability, requiring that a satellite orbiting that planet must remain within an orbital radius of ∼138,000 km in order to remain bound on astronomically long timescales.

Heller & Barnes (2013) consider the possibility of habitable exomoons orbiting the super-Earth Kepler-22b and the gas giant planet candidate KOI211.01. By considering the influence of tidal heating on the potential satellites of these planets, they reach the conclusion that "If either planet hosted a satellite at a distance greater than 10 planetary radii, then this could indicate the presence of a habitable moon." If we assume that GJ 832c is a predominantly rocky/metallic object, then we can obtain a rough estimate of its radius by following Seager et al. (2007). For a silicaceous composition, given a mass of approximately 5 $M_{\oplus}$, it seems likely that GJ 832c would have a radius approximately 50% greater than that of the Earth, or approximately 10,000 km. We can therefore determine a rough inner-edge to the circumplanetary habitable zone for GJ 832c, at approximately 10 times this value. In other words, for GJ 832c to host a habitable exomoon potentially formed by means of a giant collision during the latter stages of planet formation, such a satellite would most likely have to orbit between ∼100,000 and ∼138,000 km—a very narrow range. Although the idea of a habitable exomoon companion to GJ 832c is certainly interesting, the odds seem stacked against the existence of such an object.

4.3. Conclusions

We have combined high-precision radial-velocity data from three telescopes to detect a super-Earth (5.4 ± 1.0 $M_{\oplus}$) orbiting GJ 832 near the inner edge of the habitable zone. We attribute this detection to two key differences from the Bonfils et al. (2013a) analysis. The first is that our Bayesian techniques are better at picking out weak signals; this was powerfully demonstrated by Tuomi & Anglada-Escudé (2013), who used this approach for the GJ 163 system and obtained results consistent with Bonfils et al. (2013a) with only 35% of the HARPS data used in the discovery work. The second is that the HARPS-TERRA velocities are more sensitive to planet c than the velocities derived by the HARPS team in Bonfils et al. (2013a); Anglada-Escudé & Butler (2012) showed that HARPS-TERRA produces better velocities for M dwarfs.

Given GJ 832's close proximity, it is bright enough for high contrast imaging (Salter et al. 2014), even though it is an M dwarf. However, due to its likely old, though uncertain, age, even GJ 832b (0.63 $M_{\rm Jup}$) would not be bright enough to be detected by the current state-of-the-art instruments such as the Gemini Planet Imager on Gemini South (Macintosh et al. 2008). With a rare Jupiter analog and a potentially rocky inner planet, the GJ 832 system can be considered a scaled-down version of our solar system. With this in mind, it would be interesting to see if that analogy continues beyond the planetary members of the system to the debris. There is a growing body of work, based on *Spitzer* and *Herschel* observations, revealing correlations between the presence of debris disks and planets (Wyatt et al. 2012; Maldonado et al. 2012; Bryden et al. 2013, e.g.,). As GJ 832 is very nearby (4.95 pc), it is an ideal candidate for future imaging efforts to search for debris disks akin to our own Edgeworth–Kuiper belt and main asteroid belt. Recent work by Marshall et al. (2014) showed a correlation between low (sub-solar) metallicity, low-mass planets, and an elevated incidence of debris from *Herchel* data and radial-velocity results. As GJ 832 is quite metal poor ([Fe/H] $= -0.3$), it would thus appear to be a promising target for debris detection. Future observations of GJ 832 hold the promise to yield further secrets from this intriguing system.

Circumstellar debris discs around mature stars are the byproduct of a planetesimal formation process, composed of icy and rocky bodies ranging from micron-sized grains to kilometer-sized asteroids (see reviews by, e.g., Wyatt 2008; Krivov 2010; Moro-Martin 2013). The dust we actually observe is continually replenished in the disk through the collisional grinding of planetesimals as the grains are much shorter lived than the age of the host star, being removed by radiative processes and

[15] We note that the m sin i determined from radial velocity measurements would actually be the total mass of the exoplanet in question, plus any moons it hosts. For example, if GJ 832c hosts a moon with 20% of its own mass, then the planet mass would actually be only 0.8 times the m sin i given in Table 9.

collisional destruction (Backman & Paresce 1993). Since planets are believed to be produced through the hierarchical growth of planetesimals from smaller bodies and dust grains are produced through their collisional destruction, we expect the two phenomena to be linked. The solar system represents one outcome of the planet formation process, comprising four telluric planets, four giant planets, and two debris belts—the inner, warm Asteroid belt at 3 AU (Backman et al. 1995) and the outer, cold Edgeworth–Kuiper belt at 30 AU (Vitense et al. 2012). We detect thermal emission from warm dust around 2% ± 2% of Sun-like stars (Trilling et al. 2008) and cold dust around 20% ± 2% of Sun-like stars (Eiroa et al. 2013); such measurements are limited by sensitivity particularly for the warm dust. By comparison, the solar system's debris disk is typically faint, expected to lie in the bottom few percent of disk systems (Greaves & Wyatt 2010), and currently beyond the reach of direct detection by ground or satellite observatories. Around other stars, many host infrared excesses with two characteristic temperatures, typically at ∼150 K and ∼50 K (Morales et al. 2011). Drawing an analogy to the solar system, disks with two temperature components are interpreted as being the product of physically distinct debris belts at different orbital radii. Due to the tendency of dust to migrate away from the debris belt where it was created (Krivov et al. 2008), the presence of more or less narrow debris rings around a star has been attributed to the existence of unseen planet(s) shepherding the dust and confining its radial location through dynamical interaction, creating observable warps, clumps, gaps, and asymmetries in the disk (Moro-Martín et al. 2007; Morales et al. 2009). Several such cases of planets interacting with a debris disk have now been proposed, with candidate planets identified through direct imaging searches around several of the stars (e.g., Vega, Wyatt 2003; Beta Pic, Lagrange et al. 2010; HD 95086, Rameau et al. 2013). Indeed, planet–disk interaction has been vital in the formation and evolution of life on Earth, with minor body collisions providing both a late veneer of volatile material to the Earth's surface (O'Brien et al. 2006), the migration of Jupiter thought to be responsible for the late heavy bombardment at ∼800 Myr (Gomes et al. 2005), and subsequent infrequent catastrophic bombardment drastically altering the climate during the history of the solar system (Covey 1994; Toon et al. 1997; Feulner 2009). Therefore, any discussion of the potential habitability of an exoplanet should consider the possibility of volatile material delivery to a planet located in the habitable zone from remnant material located elsewhere in the system.

This research is supported by Australian Research Council grants DP0774000 and DP130102695. Australian access to the Magellan Telescopes was supported through the National Collaborative Research Infrastructure Strategy of the Australian Federal Government. This research has made use of NASA's Astrophysics Data System (ADS) and the SIMBAD database, operated at CDS, Strasbourg, France. This research has also made use of the Exoplanet Orbit Database and the Exoplanet Data Explorer at exoplanets.org (Wright et al. 2011).

REFERENCES

Albrecht, S., Winn, J. N., Butler, R. P., et al. 2012, ApJ, 744, 189
Albrecht, S., Winn, J. N., Johnson, J. A., et al. 2011, ApJ, 738, 50
Anglada-Escudé, G., Arriagada, P., Vogt, S. S., et al. 2012, ApJL, 751, L16
Anglada-Escudé, G., & Butler, R. P. 2012, ApJS, 200, 15
Anglada-Escudé, G., Tuomi, M., Gerlach, E., et al. 2013, A&A, 556, A126
Arriagada, P., Anglada-Escudé, G., Butler, R. P., et al. 2013, ApJ, 771, 42
Backman, D. E., Dasgupta, A., & Stencel, R. E. 1995, ApJL, 450, L35
Backman, D. E., & Paresce, F. 1993, in Protostars and Planets III, ed. E. H. Levy & J. I. Lunine (Tucson, AZ: Univ. of Arizona), 1253
Bailey, J., Butler, R. P., Tinney, C. G., et al. 2009, ApJ, 690, 743
Ballard, S., Charbonneau, D., Fressin, F., et al. 2013, ApJ, 773, 98
Baluev, R. V. 2013, MNRAS, 429, 2052
Barnes, J. R., Jenkins, J. S., Jones, H. R. A., et al. 2012, MNRAS, 424, 591
Batalha, N. M., Rowe, J. F., Bryson, S. T., et al. 2013, ApJS, 204, 24
Bean, J. L., Seifahrt, A., Hartman, H., et al. 2010, ApJ, 713, 410
Bennett, D. P., Rhie, S. H., Nikolaev, S., et al. 2010, ApJ, 713, 837
Benz, W., Slattery, W. L., & Cameron, A. G. W. 1986, Icar, 66, 515
Bonfils, X., Delfosse, X., Udry, S., et al. 2013a, A&A, 549, A109
Bonfils, X., Lo Curto, G., Correia, A. C. M., et al. 2013b, A&A, 556, A110
Borucki, W. J., Agol, E., Fressin, F., et al. 2013, Sci, 340, 587
Borucki, W. J., Koch, D., Basri, G., et al. 2010, Sci, 327, 977
Borucki, W. J., Koch, D. G., Basri, G., et al. 2011, ApJ, 736, 19
Borucki, W. J., Koch, D. G., Batalha, N., et al. 2012, ApJ, 745, 120
Boyajian, T. S., von Braun, K., van Belle, G., et al. 2012, ApJ, 757, 112
Bryden, G., Krist, J. E., Stapelfeldt, K. R., et al. 2013, BAAS, 221, 144.24
Butler, R. P., Johnson, J. A., Marcy, G. W., et al. 2006, PASP, 118, 1685
Butler, R. P., Marcy, G. W., Williams, E., et al. 1996, PASP, 108, 500
Canup, R. M. 2004, Icar, 168, 433
Canup, R. M. 2005, Sci, 307, 546
Casagrande, L., Flynn, C., & Bessell, M. 2008, MNRAS, 389, 585
Correia, A. C. M., & Laskar, J. 2009, Icar, 201, 1
Covey, C. 1994, GPC, 9, 263
Crane, J. D., Shectman, S. A., & Butler, R. P. 2006, Proc. SPIE, 6269, 96
Crane, J. D., Shectman, S. A., Butler, R. P., Thompson, I. B., & Burley, G. S. 2008, Proc. SPIE, 7014, 238
Crane, J. D., Shectman, S. A., Butler, R. P., et al. 2010, Proc. SPIE, 7735, 170
Cuntz, M., Quarles, B., Eberle, J., & Shukayr, A. 2013, PASA, 30, 33
Delfosse, X., Bonfils, X., Forveille, T., et al. 2013, A&A, 553, A8
Diego, F., Charalambous, A., Fish, A. C., & Walker, D. D. 1990, Proc. SPIE, 1235, 562
Döllinger, M. P., Hatzes, A. P., Pasquini, L., et al. 2007, A&A, 472, 649
Eiroa, C., Marshall, J. P., Mora, A., et al. 2013, A&A, 555, A11
Endl, M., Cochran, W. D., Kürster, M., et al. 2006, ApJ, 649, 436
Feulner, G. 2009, IJAsB, 8, 207
Forgan, D., & Kipping, D. 2013, MNRAS, 432, 2994
Gaudi, B. S., Bennett, D. P., Udalski, A., et al. 2008, Sci, 319, 927
Gomes, R., Levison, H. F., Tsiganis, K., & Morbidelli, A. 2005, Natur, 435, 466
Gould, A., Dong, S., Gaudi, B. S., et al. 2010, ApJ, 720, 1073
Gray, R. O., Corbally, C. J., Garrison, R. F., et al. 2006, AJ, 132, 161
Greaves, J. S., & Wyatt, M. C. 2010, MNRAS, 404, 1944
Haario, H., Laine, M., Mira, A., & Saksman, E. 2006, Stat. Comput., 16, 339
Haario, H., Saksman, E., & Tamminen, J. 2001, Bernoulli, 7, 223
Haldane, J. B. S. 1928, Possible Worlds and Other Essays, 286
Hastings, W. 1970, Biometrika, 57, 97
Hatzes, A. P., Guenther, E. W., Endl, M., et al. 2005, A&A, 437, 743
Heath, M. J., Doyle, L. R., Joshi, M. M., & Haberle, R. M. 1999, OLEB, 29, 405
Heller, R. 2012, A&A, 545, L8
Heller, R., & Barnes, R. 2013, AsBio, 13, 18
Horner, J., & Jones, B. W. 2008, IJAsB, 7, 251
Horner, J., & Jones, B. W. 2009, IJAsB, 8, 75
Horner, J., & Jones, B. W. 2010, IJAsB, 9, 273
Horner, J., Jones, B. W., & Chambers, J. 2010, IJAsB, 9, 1
Howard, A. W. 2013, Sci, 340, 572
Howard, A. W., Johnson, J. A., Marcy, G. W., et al. 2010, ApJ, 721, 1467
Howard, A. W., Marcy, G. W., Bryson, S. T., et al. 2012, ApJS, 201, 15
Jefferys, W. H., Fitzpatrick, M. J., & McArthur, B. E. 1988, CeMec, 41, 39
Jenkins, J. S., Jones, H. R. A., Tinney, C. G., et al. 2006, MNRAS, 372, 163
Johnson, J. A., Marcy, G. W., Fischer, D. A., et al. 2006, ApJ, 652, 1724
Jones, H. R. A., Butler, R. P., Tinney, C. G., et al. 2010, MNRAS, 403, 1703
Kane, S. R., Barclay, T., & Gelino, D. M. 2013, ApJL, 770, L20
Kant, I. 1755, Allgemeine Naturgeschichte und Theorie des Himmels. Zeitz, Bei W. Webel, 1798. Neue aufl.
Kass, R. E., & Raftery, A. E. 1995, J. Am. Stat. Assoc., 430, 773
Kasting, J. F. 1988, Icar, 74, 472
Kasting, J. F., Whitmire, D. P., & Reynolds, R. T. 1993, Icar, 101, 108
Kipping, D. M., Forgan, D., Hartman, J., et al. 2013, ApJ, 777, 134
Kopparapu, R. K., Ramirez, R. M., SchottelKotte, J., et al. 2014, ApJL, 787, L29
Krivov, A. V. 2010, RAA, 10, 383
Krivov, A. V., Müller, S., Löhne, T., & Mutschke, H. 2008, ApJ, 687, 608
Kürster, M., Schmitt, J. H. M. M., Cutispoto, G., & Dennerl, K. 1997, A&A, 320, 831

Lagrange, A.-M., Bonnefoy, M., Chauvin, G., et al. 2010, Sci, 329, 57
Laplace, P. S., & Young, T. (ed.) 1832, Elementary Illustrations of the Celestial Mechanics of Laplace (London: J. Murray).
Lestrade, J.-F., Matthews, B. C., Sibthorpe, B., et al. 2012, A&A, 548, A86
Lomb, N. R. 1976, Ap&SS, 39, 447
Macintosh, B. A., Graham, J. R., Palmer, D. W., et al. 2008, Proc. SPIE, 7015, 31
Mahadevan, S., Ramsey, L., Bender, C., et al. 2012, Proc. SPIE, 8446, 1
Makarov, V. V., & Berghea, C. 2014, ApJ, 780, 124
Maldonado, J., Eiroa, C., Villaver, E., Montesinos, B., & Mora, A. 2012, A&A, 541, A40
Marshall, J. P., Moro-Martín, A., Eiroa, C., et al. 2014, A&A, 565, A15
Matthews, B. C., Sibthorpe, B., Kennedy, G., et al. 2010, A&A, 518, L135
Mayor, M., Bonfils, X., Forveille, T., et al. 2009, A&A, 507, 487
Metropolis, N., Rosenbluth, A. W., Rosenbluth, M. N., et al. 1953, JChPh, 21, 1087
Morales, F. Y., Rieke, G. H., Werner, M. W., et al. 2011, ApJL, 730, L29
Morales, F. Y., Werner, M. W., Bryden, G., et al. 2009, ApJ, 699, 1067
Moro-Martin, A. 2013, Planets, Stars and Stellar Systems. Volume 3: Solar and Stellar Planetary Systems (Berlin: Springer), 431
Moro-Martín, A., Carpenter, J. M., Meyer, M. R., et al. 2007, ApJ, 658, 1312
Neubauer, D., Vrtala, A., Leitner, J. J., Gertrude Firneis, M., & Hitzenberger, R. 2012, P&SS, 73, 397
Newton, M. A., & Raftery, A. E. 1994, JRSS B, 56, 3
Niedzielski, A., Goździewski, K., Wolszczan, A., et al. 2009, ApJ, 693, 276
O'Brien, D. P., Greenberg, R., & Richardson, J. E. 2006, Icar, 183, 79
Petigura, E. A., Howard, A. W., & Marcy, G. W. 2013, PNAS, 110, 19273
Queloz, D., Henry, G. W., Sivan, J. P., et al. 2001, A&A, 379, 279
Quirrenbach, A., Amado, P. J., Mandel, H., et al. 2010, Proc. SPIE, 7735, 37
Rameau, J., Chauvin, G., Lagrange, A.-M., et al. 2013, ApJL, 772, L15
Robertson, P., Endl, M., Cochran, W. D., MacQueen, P. J., & Boss, A. P. 2013, ApJ, 774, 147
Robertson, P., Endl, M., Cochran, W. D., et al. 2012a, ApJ, 749, 39
Robertson, P., Horner, J., Wittenmyer, R. A., et al. 2012b, ApJ, 754, 50
Rowe, J. F., Bryson, S. T., Marcy, G. W., et al. 2014, ApJ, 784, 45
Salter, G. S., Tinney, C. G., Wittenmyer, R. A., et al. 2014, in IAU Symp. 299, Exploring the Formation and Evolution of Planetary Systems (Cambridge: Cambridge Univ. Press), 66
Sato, B., Kambe, E., Takeda, Y., et al. 2005, PASJ, 57, 97
Scargle, J. D. 1982, ApJ, 263, 835
Schiavon, R. P., Barbuy, B., & Singh, P. D. 1997, ApJ, 484, 499
Seager, S., Kuchner, M., Hier-Majumder, C. A., & Militzer, B. 2007, ApJ, 669, 1279
Selsis, F., Kasting, J. F., Levrard, B., et al. 2007, A&A, 476, 1373
Setiawan, J., Pasquini, L., da Silva, L., von der Lühe, O., & Hatzes, A. 2003, A&A, 397, 1151
Tadeu dos Santos, M., Silva, G. G., Ferraz-Mello, S., & Michtchenko, T. A. 2012, CeMDA, 113, 49
Tarter, J. C., Backus, P. R., Mancinelli, R. L., et al. 2007, AsBio, 7, 30
Tinney, C. G., Wittenmyer, R. A., Butler, R. P., et al. 2011, ApJ, 732, 31
Toon, O. B., Zahnle, K., Morrison, D., Turco, R. P., & Covey, C. 1997, RvGeo, 35, 41
Trilling, D. E., Bryden, G., Beichman, C. A., et al. 2008, ApJ, 674, 1086
Tuomi, M. 2011, A&A, 528, L5
Tuomi, M. 2014, MNRAS, 440, L1
Tuomi, M., & Anglada-Escudé, 2013, A&A, 556, A111
Tuomi, M., Anglada-Escudé, G., Gerlach, E., et al. 2013a, A&A, 549, A48
Tuomi, M., Jones, H. R. A., Barnes, J. R., Anglada-Escudé, G., & Jenkins, J. S. 2014, MNRAS, 441, 1545
Tuomi, M., Jones, H. R. A., Jenkins, J. S., et al. 2013b, A&A, 551, A79
Valenti, J. A., Butler, R. P., & Marcy, G. W. 1995, PASP, 107, 966
van Leeuwen, F. 2007, A&A, 474, 653
Vitense, C., Krivov, A. V., Kobayashi, H., & Lohne, T. 2012, A&A, 540, A30
Vogt, S. S., Butler, R. P., & Haghighipour, N. 2012, AN, 333, 561
Vogt, S. S., Butler, R. P., Rivera, E. J., et al. 2010, ApJ, 723, 954
von Braun, K., Boyajian, T. S., Kane, S. R., et al. 2011, ApJL, 729, L26
Wittenmyer, R. A., Endl, M., Cochran, W. D., et al. 2006, AJ, 132, 177
Wittenmyer, R. A., Endl, M., Wang, L., et al. 2011a, ApJ, 743, 184
Wittenmyer, R. A., Tinney, C. G., O'Toole, S. J., et al. 2011b, ApJ, 727, 102
Wittenmyer, R. A., Horner, J., Marshall, J. P., Butters, O. W., & Tinney, C. G. 2012a, MNRAS, 419, 3258
Wittenmyer, R. A., Horner, J., Tinney, C. G., et al. 2014a, ApJ, 783, 103
Wittenmyer, R. A., Horner, J., Tuomi, M., et al. 2012b, ApJ, 753, 169
Wittenmyer, R. A., Tan, X., Lee, M. H., et al. 2014b, ApJ, 780, 140
Wright, J. T., Fakhouri, O., Marcy, G. W., et al. 2011, PASP, 123, 412
Wyatt, M. C. 2003, ApJ, 598, 1321
Wyatt, M. C. 2008, ARA&A, 46, 339
Wyatt, M. C., Kennedy, G., Sibthorpe, B., et al. 2012, MNRAS, 424, 1206
Yang, J., Boué, G., Fabrycky, D. C., & Abbot, D. S. 2014, ApJL, 787, L2
Zechmeister, M., & Kürster, M. 2009, A&A, 496, 577
Zechmeister, M., Kürster, M., Endl, M., et al. 2013, A&A, 552, A78